

# Continuously tunable microdroplet-laser in a microfluidic channel

Sindy K. Y. Tang,<sup>1</sup> Ratmir Derda,<sup>1,2</sup> Qimin Quan,<sup>2,3</sup> Marko Lončar,<sup>3</sup>  
and George M. Whitesides<sup>1,\*</sup>

<sup>1</sup>Department of Chemistry and Chemical Biology, Wyss Institute for  
Biologically Inspired Engineering, Harvard University, Cambridge, Massachusetts 02138, USA

<sup>2</sup>These authors contributed equally to this work.

<sup>3</sup>School of Engineering and Applied Sciences, Harvard University, Cambridge, Massachusetts 02138, USA

\*gwhitesides@gmwhgroup.harvard.edu

**Abstract:** This paper describes the generation and optical characterization of a series of dye-doped droplet-based optical microcavities with continuously decreasing radius in a microfluidic channel. A flow-focusing nozzle generated the droplets (~21  $\mu\text{m}$  in radius) using benzyl alcohol as the disperse phase and water as the continuous phase. As these drops moved down the channel, they dissolved, and their size decreased. The emission characteristics from the drops could be matched to the whispering gallery modes from spherical micro-cavities. The wavelength of emission from the drops changed from 700 to 620 nm as the radius of the drops decreased from 21  $\mu\text{m}$  to 7  $\mu\text{m}$ . This range of tunability in wavelengths was larger than that reported in previous work on droplet-based cavities.

©2011 Optical Society of America

**OCIS codes:** (140.2050) Dye lasers; (140.3948) Microcavity devices.

---

## References and links

1. S. C. Hill, and R. E. Benner, "Morphology-dependent resonances," in *Optical Effects Associated with Small Particles*, R. K. Chang, and P. W. Barber, eds. (World Scientific Publishing Co., 1988), pp. 3–61.
2. R. K. Chang, and A. J. Campillo, *Optical Processes in Microcavities* (World Scientific Publishing Co., 1996).
3. H. M. Tzeng, K. F. Wall, M. B. Long, and R. K. Chang, "Laser emission from individual droplets at wavelengths corresponding to morphology-dependent resonances," *Opt. Lett.* **9**(11), 499–501 (1984).
4. H. M. Tzeng, K. F. Wall, M. B. Long, and R. K. Chang, "Evaporation and condensation rates of liquid droplets deduced from structure resonances in the fluorescence spectra," *Opt. Lett.* **9**(7), 273–275 (1984).
5. H. M. Tzeng, M. B. Long, R. K. Chang, and P. W. Barber, "Laser-induced shape distortions of flowing droplets deduced from morphology-dependent resonances in fluorescence spectra," *Opt. Lett.* **10**(5), 209–211 (1985).
6. S. K. Y. Tang, Z. Li, A. R. Abate, J. J. Agresti, D. A. Weitz, D. Psaltis, and G. M. Whitesides, "A multi-color fast-switching microfluidic droplet dye laser," *Lab Chip* **9**(19), 2767–2771 (2009).
7. J. Schäfer, J. P. Mondia, R. Sharma, Z. H. Lu, A. S. Susha, A. L. Rogach, and L. J. Wang, "Quantum dot microdroplet laser," *Nano Lett.* **8**(6), 1709–1712 (2008).
8. M. Saito, H. Shimatani, and H. Naruhashi, "Tunable whispering gallery mode emission from a microdroplet in elastomer," *Opt. Express* **16**(16), 11915–11919 (2008).
9. S. X. Qian, J. B. Snow, H. M. Tzeng, and R. K. Chang, "Lasing droplets: highlighting the liquid-air interface by laser emission," *Science* **231**(4737), 486–488 (1986).
10. M. M. Mazumder, G. Chen, P. J. Kindlmann, R. K. Chang, and J. B. Gillespie, "Temperature-dependent wavelength shifts of dye lasing in microdroplets with a thermochromic additive," *Opt. Lett.* **20**(16), 1668–1670 (1995).
11. M. M. Mazumder, G. Chen, R. K. Chang, and J. B. Gillespie, "Wavelength shifts of dye lasing in microdroplets: effect of absorption change," *Opt. Lett.* **20**(8), 878–880 (1995).
12. H. B. Lin, A. L. Huston, B. L. Justus, and A. J. Campillo, "Some characteristics of a droplet whispering-gallery-mode laser," *Opt. Lett.* **11**(10), 614–616 (1986).
13. H. B. Lin, J. D. Eversole, and A. J. Campillo, "Spectral properties of lasing microdroplets," *J. Opt. Soc. Am. B* **9**(1), 43–50 (1992).
14. A. Kiraz, A. Kurt, M. A. Dündar, and A. L. Demirel, "Simple largely tunable optical microcavity," *Appl. Phys. Lett.* **89**(8), 081118 (2006).
15. C. G. Garrett, W. Kaiser, and W. L. Bond, "Stimulated emission into optical whispering modes of spheres," *Phys. Rev.* **124**(6), 1807–1809 (1961).
16. G. Chen, M. M. Mazumder, Y. R. Chemla, A. Serpenguzel, R. K. Chang, and S. C. Hill, "Wavelength variation of laser emission along the entire rim of slightly deformed microdroplets," *Opt. Lett.* **18**(23), 1993–1995 (1993).

17. A. J. Campillo, J. D. Eversole, and H. B. Lin, "Cavity quantum electrodynamic enhancement of stimulated emission in microdroplets," *Phys. Rev. Lett.* **67**(4), 437–440 (1991).
18. P. Garstecki, I. Gitlin, W. DiLuzio, G. M. Whitesides, E. Kumacheva, and H. A. Stone, "Formation of monodisperse bubbles in a microfluidic flow-focusing device," *Appl. Phys. Lett.* **85**(13), 2649–2651 (2004).
19. Z. H. Nie, M. S. Seo, S. Q. Xu, P. C. Lewis, M. Mok, E. Kumacheva, G. M. Whitesides, P. Garstecki, and H. A. Stone, "Emulsification in a microfluidic flow-focusing device: effect of the viscosities of the liquids," *Microfluid. Nanofluid.* **5**, 585–594 (2008).
20. P. Garstecki, H. A. Stone, and G. M. Whitesides, "Mechanism for flow-rate controlled breakup in confined geometries: a route to monodisperse emulsions," *Phys. Rev. Lett.* **94**(16), 164501 (2005).
21. S. L. Anna, N. Bontoux, and H. A. Stone, "Formation of dispersions using "flow focusing" in microchannels," *Appl. Phys. Lett.* **82**(3), 364–366 (2003).
22. J. C. McDonald, D. C. Duffy, J. R. Anderson, D. T. Chiu, H. Wu, O. J. Schueller, and G. M. Whitesides, "Fabrication of microfluidic systems in poly(dimethylsiloxane)," *Electrophoresis* **21**(1), 27–40 (2000).
23. P. Garstecki, M. J. Fuerstman, H. A. Stone, and G. M. Whitesides, "Formation of droplets and bubbles in a microfluidic T-junction-scaling and mechanism of break-up," *Lab Chip* **6**(3), 437–446 (2006).
24. S. K. Y. Tang, C. A. Stan, and G. M. Whitesides, "Dynamically reconfigurable liquid-core liquid-cladding lens in a microfluidic channel," *Lab Chip* **8**(3), 395–401 (2008).
25. W. Lee, L. M. Walker, and S. L. Anna, "Role of geometry and fluid properties in droplet and thread formation processes in planar flow focusing," *Phys. Fluids* **21**(3), 032103 (2009).
26. The polydispersity is calculated as  $s/d$ , where  $s$  is the standard deviation in drop diameters, and  $d$  is the average drop diameter. We imaged 60 drops and used a custom-made Matlab program to extract the droplet diameters.
27. To prepare the saturated solutions, we mixed 1:1 ratio of benzyl alcohol and water. We stirred the mixture for 30 min at 60 degree C. We then centrifuged the mixture, and extracted the top phase (water saturated with benzyl alcohol) and bottom phase (benzyl alcohol saturated with water).
28. J. I. Park, Z. Nie, A. Kumachev, and E. Kumacheva, "A microfluidic route to small CO<sub>2</sub> microbubbles with narrow size distribution," *Soft Matter* **6**(3), 630–634 (2010).
29. C. C. Lam, P. T. Leung, and K. Young, "Explicit asymptotic formulas for the positions, widths, and strengths of resonances in Mie scattering," *J. Opt. Soc. Am. B* **9**(9), 1585–1592 (1992).
30. J. D. Eversole, H. B. Lin, A. L. Huston, A. J. Campillo, P. T. Leung, S. Y. Liu, and K. Young, "High-precision identification of morphology-dependent resonances in optical processes in microdroplets," *J. Opt. Soc. Am. B* **10**(10), 1955–1968 (1993).
31. J. Clausell-Tormos, D. Lieber, J.-C. Baret, A. El-Harrak, O. J. Miller, L. Frenz, J. Blouwolff, K. J. Humphry, S. Köster, H. Duan, C. Holtze, D. A. Weitz, A. D. Griffiths, and C. A. Merten, "Droplet-based microfluidic platforms for the encapsulation and screening of Mammalian cells and multicellular organisms," *Chem. Biol.* **15**(5), 427–437 (2008).
32. J. A. Stratton, *Electromagnetic Theory* (McGraw-Hill, 1941).

## 1. Introduction

In a micro-spherical cavity, light is confined by total internal reflections at the interface between the microsphere and the medium that surrounds it. Electromagnetic waves—coupled into the cavity or emitted from a gain medium inside the cavity—that meet the requirements for constructive interference form cavity resonances called whispering gallery modes (WGMs). The energy stored in the cavity at these frequencies increases, due to large quality factors of these resonances. We and others have demonstrated enhancement of light and lasing in WGMs from microcavities made of droplets [1–17]. Microdroplets—with their small sizes, and with their surfaces made spherical and smoothed by surface tension—are effective optical microcavities. Microfluidics technology (based on flow-focusing nozzles, T-junctions, and other structures) allows convenient generation of large numbers of monodisperse drops and bubbles at rates up to  $> 10$  kHz [18]. The diameters of drops and bubbles produced are usually in the range of tens of microns [19–21]. This length scale is well-suited for studies of whispering gallery modes in the visible and near-infrared wavelengths. By combining two microfluidic T-junctions for alternate generation of drops containing different types of dye solutions, we demonstrated switching of lasing wavelengths between 580 nm and 680 nm at frequencies up to 3.6 kHz, the fastest for a reported dye laser [6]. These drop-based dye lasers have the potential to be useful in combination with other microfluidic components for on-chip spectroscopy applications.

This paper extends the idea of wavelength tuning in droplet-based dye lasers by using droplet cavities whose size decreases continuously after generation. We formed drops using two liquids—benzyl alcohol for the drops, water for the carrier fluid—that were partially miscible with each other. As the drops traveled downstream, they dissolved into the carrier fluid and decreased in size. The time for the drops to dissolve was similar to the residence

time of the drops in the channel. A large range of sizes of drops was therefore present in the channel at any time. At fixed positions in the channel, the size of the drops was fixed. By positioning the excitation laser at different parts of the channel, we were able to interrogate the optical properties of droplet cavities possessing different sizes.

We observed that the emission wavelengths from the droplet cavities changed over a large range ( $\sim 80$  nm) as the radius of the cavities decreased from  $21\ \mu\text{m}$  to  $7\ \mu\text{m}$ . This range was larger than that reported in previous studies of droplets evaporating in air ( $< 10$  nm) [4,14]. Selection of the size of the droplets according to their position in the channel made it possible to select the wavelengths of emission over this  $\sim 80$  nm range. The rate at which wavelengths could be tuned or selected was relatively slow in the device we describe ( $\sim$ seconds), but could be reduced to milliseconds using a rapidly steerable excitation beam. As the drops decreased in size, the refractive index of the drops and the concentration of dye solutions in the drops also changed. We show that these effects were, however, much smaller than that due to the decrease in the size of the drops in causing the change in emission characteristics from the drops.

To our knowledge, we were the first to report the use of dissolution of liquid drops into a second liquid to achieve a large range in the size of the drops and in their emission wavelengths. The use of dissolution of one liquid into another liquid has major advantages over previous systems based on drops evaporating in air: (i) Liquid-liquid systems are compatible with existing microfluidics platform. It is, therefore, simple to integrate droplet microcavities with other micro-components for the development of practical applications. (ii) It is easy to control the paths of flow of drops suspended in another liquid in arbitrary directions in a microchannel. This control facilitates the miniaturization of the system since a long microchannel can be intertwined to minimize the physical area of the microfluidic chip. It is difficult, on the other hand, to direct the flow of drops in air in arbitrary directions within small areas. (iii) There are many surfactants that can stabilize droplets in liquid-liquid systems; these drops do not coalesce under close-packed conditions and can be stored, and re-used, if desired, over long periods of time (days to months). Drops in liquid-liquid systems have the potential to be useful for long-term monitoring of physical or biochemical reactions that occur inside or outside of the drops. Stabilization and storage of drops in air is, in general, very difficult.

## 2. Experimental design

### 2.1 Microchannel design

We fabricated a flow-focusing nozzle (FFN) [21] to generate droplets in poly(dimethylsiloxane) (PDMS) using soft lithography [22]. Other structures for generating drops, such as T-junctions [23], could also be used. The height of the channel was  $40\ \mu\text{m}$ . The length of the channel was 16 cm, and the width of the channel decreased from  $60\ \mu\text{m}$  to  $20\ \mu\text{m}$  continuously (Fig. 1a). Using channels with tapered width kept the drops centered as they decreased in size. The long channel was necessary to allow sufficient time for the drops to dissolve into the carrier fluid, and, thus, to change size sufficiently to change the wavelength of emission over a useful range. In the simple constructed device we used, we were unable to cause fluids to flow through a channel longer than 16 cm due to the high fluidic resistance to fluid flow. At the pressure that would have been required to produce usefully rapid flows through long channels, the tubings used to bring fluids to the FFN and channel detached from the inlets of the PDMS device. It should be possible to solve this problem by using a different method of connection to the channel, a microfluidic system of different design, or by applying vacuum to the outlet of the channel to assist the flow in channels longer than 16 cm. We have not demonstrated these capabilities in this work.

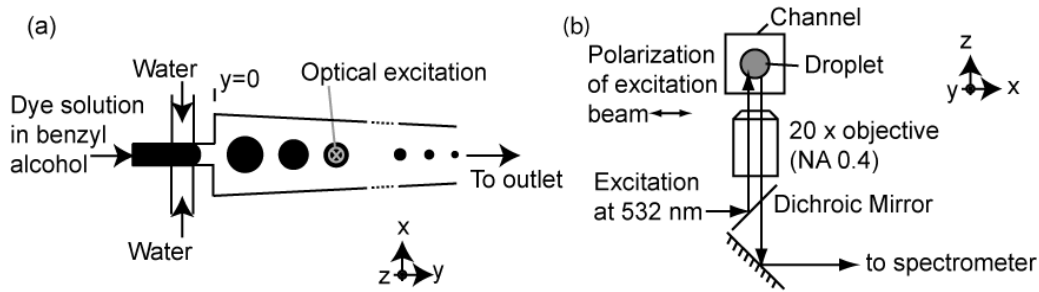


Fig. 1. a) shows a schematic diagram of the droplet laser. The width of the channel at the flow-focusing nozzle was  $15\ \mu\text{m}$ . The width of the channel was  $60\ \mu\text{m}$  at  $y = 0$ , and narrowed to  $20\ \mu\text{m}$  at  $y = 16\ \text{cm}$ . The height of the channel (in the  $z$ -direction) was  $43\ \mu\text{m}$ . Drops containing  $1\ \text{mM}$  solution of rhodamine 640 perchlorate in benzyl alcohol dissolved into water as they travelled in the channel, and their sizes decreased. The concentration of rhodamine increased as the volume of the drops decreased. This effect on the emission spectrum from the droplet cavities was insignificant (see text). b) The droplets were optically excited by a pulsed frequency-doubled Nd:YAG at repetition rate of  $1\ \text{kHz}$ , much higher than the rate of generation of drops ( $\sim 125$  drops/second). The excitation beam was directed perpendicular to the plane of the microchannel (in the  $z$ -direction). The optical output from the drops was collected through an objective behind the channel in the same direction as the pump beam ( $z$ -direction). The dichroic mirror reflects light with wavelength at  $532\ \text{nm}$ , and transmits light with wavelengths  $> 532\ \text{nm}$ .

## 2.2 Choice of fluids

To form droplet microcavities, we used  $1\ \text{mM}$  solution of rhodamine 640 perchlorate in benzyl alcohol ( $n_{\text{drop}} = 1.54$ ) as the disperse phase, and water ( $n_{\text{carrier}} = 1.33$ ) with  $0.5\%$  sodium dodecyl sulfate (SDS) as the continuous phase. Rhodamine was the gain medium. SDS was necessary to facilitate stable generation of the drops, and to prevent the drops from wetting the walls of the channel. In principle, other pairs of liquids could also be used so long as they satisfy four requirements: (i) The contrast in refractive index between the drop and the carrier fluid must be sufficiently high to allow confinement of light for lasing in whispering gallery modes in droplets with radius studied. The contrast in index here was  $\Delta n = 0.21$ , and the radius of the drops was between  $21\ \mu\text{m}$  and  $7\ \mu\text{m}$ . A list of refractive indices for common liquids can be found in the supplementary information in [24]. (ii) The disperse phase must dissolve the laser dye readily. Rhodamine 640 perchlorate was soluble in benzyl alcohol up to  $0.591\ \text{g/mL}$ . (iii) The capillary number characterizing the importance of viscous forces over interfacial forces ( $\text{Ca} = u\eta/\gamma$ ,  $u$  is the characteristic speed of the liquids,  $\eta$  is dynamic viscosity of the liquids, and  $\gamma$  is the interfacial tension between the disperse and continuous phases) must be sufficiently low to allow stable generation of monodisperse drops at the FFN [25]. The Ca number in our system was about  $0.04$ . Monodispersity in the size of the drops also ensures a uniform dissolution rate of the drops, and that the drops had the same size at fixed positions downstream in the channel. The polydispersity of the drops generated by our FFN was  $< 1\%$  (Fig. 2b) [26]. (iv) The liquids must be partially miscible with each other. The solubility limit of benzyl alcohol in water was  $4\ \text{wt}\%$ , and that of water in benzyl alcohol was  $8\ \text{wt}\%$ .

We used a syringe pump to introduce liquids into the microchannel. We fixed the rates of flow of the continuous phase at  $200\ \mu\text{L h}^{-1}$ , and that of the disperse phase at  $20\ \mu\text{L h}^{-1}$  for all experiments unless stated otherwise. The drops produced by the FFN always had the same radius ( $\sim 22\ \mu\text{m}$ ). The rate of generation was constant at  $\sim 125$  drops/second; this rate could be increased to over  $1000$  drops/second, if desired, by using higher rates of flow. For some control experiments, we formed drops from benzyl alcohol that was saturated with water, in a carrier liquid of water that was saturated with benzyl alcohol. These drops did not dissolve into the carrier liquid and their size did not change as they traveled in the channel. Using this combination of liquids, we were able to study the effects of parameters such as the concentration of dye solution in the drops independent of the size of the drops [27].

### 2.3 Optical excitation and measurements

We mounted the microfluidic device on an inverted microscope (Fig. 1b). We used a pulsed, frequency-doubled Nd:YAG laser at 532 nm as the excitation source. The pump beam was coupled into the microscope and focused at the microchannel with a beam diameter of  $\sim 30$   $\mu\text{m}$ . Since the pump spot was comparable to, or larger than, the size of the drops we used, we believe the whole drop was excited relatively uniformly. The pulse width of the pump laser was 20 ns. During this time, the drop moved  $< 1$  nm; this movement should have insignificant effect on the emission spectrum. The repetition rate of the laser was 1 kHz. At this repetition rate, each drop was excited once or twice as the residence time of drops in the pump spot was between 1 to 2 ms. We did not observe photobleaching of the dye since the drops were flowing continuously and each drop was excited not more than two times. The pump laser was not synchronized with the drops; the part of the drop that was excited was not always the same. We observed small changes in the emission spectra ( $\sim 1$  nm shifts) depending on where the drop was excited. These shifts were, however, insignificant relative to the 80 nm-shift observed due to the dissolution of the drop.

To characterize the emission from the drops, we varied the pump pulse energy from 0.01 to 100  $\text{J}\cdot\text{cm}^{-2}$ . We collected light emitted from the drops using a 20x objective (numerical aperture  $\text{NA} = 0.4$ ) normal to the plane of the microchannel (in the  $z$ -direction). The light was coupled to a spectrometer for characterization using an optical fiber. Since the focal point of the excitation source was fixed in our setup, in order to select and examine drops with different sizes, we adjusted the position of the device using a manual translation stage on the microscope to bring different parts of the channel into the focus of the excitation beam.

## 3. Results and discussions

### 3.1 Generation of droplet resonators with continuously decreasing sizes

We recorded movies of the drops in the channel using a fast camera (at 5000 frames/s) and measured the radius of the drops at different locations downstream from the FFN. The drops travelled through a 16-cm long channel in  $\sim 3.5$  seconds (Fig. 2). During this time, the radius of the drops decreased from 22  $\mu\text{m}$  to less than 5  $\mu\text{m}$ . While the kinetics and mathematical model of the dissolution of droplets flowing in a narrow microchannel has not been reported, we found that the decrease in the size of the drops could be described by first-order kinetics with respect to the surface area of the droplet at a rate constant of  $0.92 \text{ s}^{-1}$  (Fig. 2d). This observation is similar to that reported for the dissolution of  $\text{CO}_2$  bubbles in a microchannel [28]. From the first-order kinetics fit, the characteristic time of dissolution, or, the time required for the size of the droplet to decrease by 50%, was  $\sim 1.5$  seconds, shorter than the residence time of drops in the channel ( $\sim 3.5$  seconds). We could, therefore, obtain a sufficiently large range of droplet sizes in the channel. We extrapolated that droplets with radius of 20  $\mu\text{m}$  would reach sub-micron size in approximately 8 seconds in our system. It was difficult to observe this decrease in radius in our experimental setup, however. At average droplet speed of 4 to 5  $\text{cm s}^{-1}$ , a 30- to 40-cm channel would be necessary to obtain sub-micron droplets; the corresponding fluidic resistance would be too high to drive fluids through this channel.

### 3.2 Identification of WGM modes from the lasing spectrum

We first characterized the optical properties from drops possessing a fixed size. For this experiment only, we increased the rate of flow of the continuous phase to 400  $\mu\text{L h}^{-1}$  and generated drops with radius  $\sim 17.4$   $\mu\text{m}$ . We measured light emitted from the drops within 50  $\mu\text{m}$  from the FFN before much dissolution of the drop occurred.

Figure 3 shows the emission characteristics from the drops when excited below and above lasing thresholds. When excited by a pump beam with power below the threshold for lasing, we observed fluorescence from the drop where the pump beam was focused (Fig. 3ai). The emission spectrum was similar to the bulk fluorescence of the dye (dashed in Fig. 3c,e). At

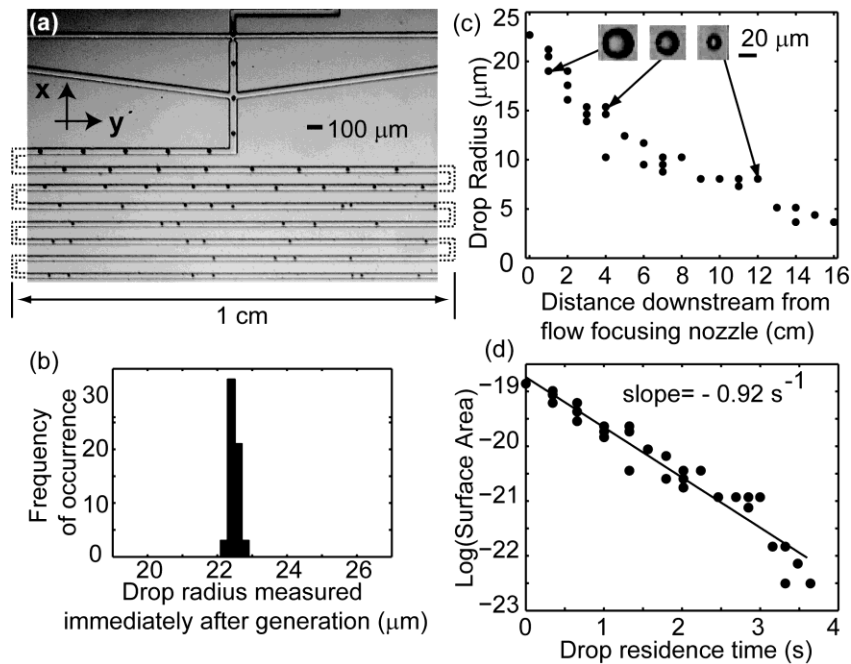


Fig. 2. a) shows a snapshot of the device during its operation. b) shows the distribution of sizes of drops generated by the flow-focusing nozzle. The polydispersity of drop sizes was less than 1% (see text). c) shows the radius of the drops at different distances down the channel. The rate of flow of the carrier fluid was  $200 \mu\text{L h}^{-1}$ , and that of the disperse phase was  $20 \mu\text{L h}^{-1}$ . The insets show images of the drops at different positions in the channel. The image of the smallest drop appears smeared because the drop was moving faster than the frame rate of the camera. d) shows the surface area of the drops as a function of their residence time in the channel. The decrease in surface area follows a first-order kinetics with rate constant  $k = -0.92 \text{ s}^{-1}$ . The  $R^2$  value for the fit was 0.94.

pump powers above the lasing threshold ( $> 2 \mu\text{J/pulse}$ , Fig. 3d), we observed a ring of high intensity around the circumference of the drop (Fig. 3aii), similar to that reported in previous droplet lasing experiments [9,15]. The emission spectrum exhibited multiple modes or peaks in intensity from  $660 \text{ nm} - 675 \text{ nm}$  (Fig. 3e). The spacing between the lasing modes was  $2.7 \text{ nm}$ , corresponding to a free spectral range (FSR) of  $\sim 1.8 \times 10^{12} \text{ Hz}$ . The spectrum in Fig. 3e is representative of emission from a single drop.

The theoretical description of the lasing conditions for WGM modes has been described previously [13] (see also Appendix Eqs. (A1), (A2)). Qualitatively, modes lase when the gain is larger than or equal to the loss due to absorption of the dyes, and radiative loss of light out of the droplet. Since the absorption and gain spectrum of rhodamine overlaps from  $\sim 550 \text{ nm}$  to  $620 \text{ nm}$  (Fig. 3c), lasing tends to occur at the long-wavelength end of the gain spectrum  $> 620 \text{ nm}$ .

WGMs from microspheres can be characterized by three numbers:  $p$ ,  $m$  and  $l$ , for both TE (transverse electric) and TM (transverse magnetic) polarizations [13]. The  $p$ ,  $m$ , and  $l$  numbers are integers, and they represent the distribution of intensity of the resonant modes inside a sphere.  $p$  indicates the number of peaks in intensity inside the sphere in the radial direction.  $m$  indicates the number of peaks along the circumference of the sphere in the direction of circulation of the WGMs, and  $l - m + 1$  indicates the number of peaks in the azimuthal direction. We compared the positions of the observed lasing modes to theoretical values calculated for passive micro-spherical resonators using explicit asymptotic formula and mode identification algorithm derived in [29,30] (Appendix Eq. (A5)). Using this algorithm, we found that these modes could be best-matched to transverse magnetic (TM) modes of a spherical cavity with radius  $R = 17.35 \mu\text{m}$ ,  $n_{\text{drop}} = 1.54$ ,  $n_{\text{carrier}} = 1.33$  with  $p = 1$ , and  $m = l =$

238 to 244. We note that this algorithm also gave other combinations of cavity radius and mode numbers that were close to our experimental data. Nevertheless, lasing in  $p = 1$  modes has been observed before [13,14]. Using Eq. (2) (to be described in section 3.3.3), we found that the wavelength at which peak lasing output power occurred for  $p = 1$  modes matched well with our experimental data; peak lasing power for modes with  $p = 2$  and 3 occurred at much shorter wavelengths than that observed (data not shown). We believe, therefore, the peaks we observed came from  $p = 1$  modes.

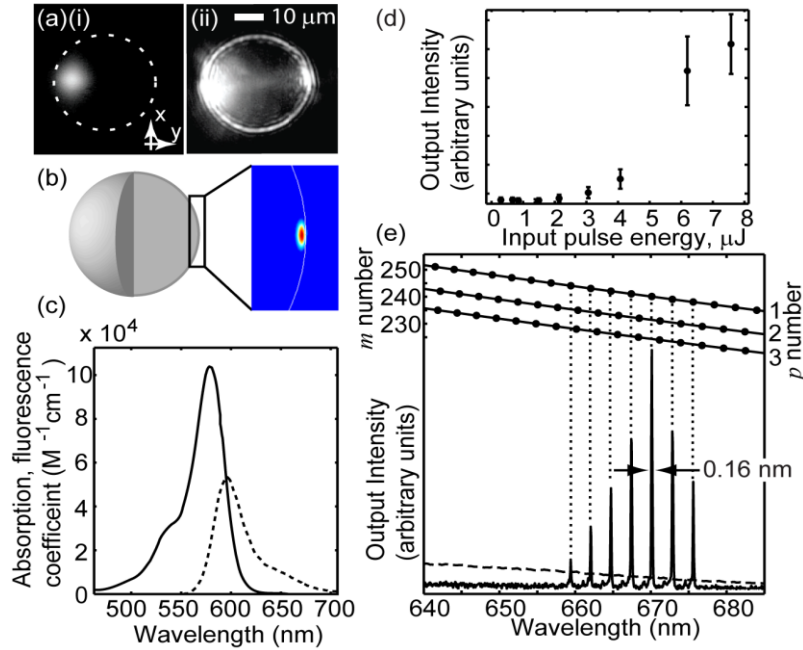


Fig. 3. a) Optical micrographs of emitted light ( $> 600$  nm) from a droplet with radius  $\sim 17.4$   $\mu\text{m}$  imaged in the  $x$ - $y$  plane when illuminated (i) by a low-power (100 mW) continuous-wave green laser with energy below lasing threshold, and (ii) by a pulsed green laser (0.24 mJ/pulse) with energy above lasing threshold. The dotted line in (a)(i) shows the outline of the drop. (b) shows a rendering image of a spherical micro-cavity and the cross-section of a WGM energy density profile ( $p = 1$ ,  $m = l = 238$ ), generated using finite element method (FEM) simulations. The radius of the cavity simulated was 17.352  $\mu\text{m}$ . The index of the cavity was 1.54, and that in the surroundings was 1.33. (c) Absorption (solid line) and fluorescence spectra (dashed line) from rhodamine 640 perchlorate in benzyl alcohol. (d) shows the output intensity from the droplet integrated over wavelengths from 650 nm to 690 nm as a function of input pulse energy. The lasing threshold was about 2  $\mu\text{J}/\text{pulse}$ . The points in this inset were averages of 14 sets of data. The error bar equals to one standard deviation. (e) Emission spectrum of a single droplet containing 1-mM solution of rhodamine 640 in benzyl alcohol at input pulse energy of 0.24 mJ/pulse, corresponding to the image in (a)(ii). The spectrum is representative of emission from a single drop. The dashed line shows the fluorescence spectrum below lasing threshold, corresponding to the image in (a)(i). The calculated WGM positions for a spherical cavity with radius = 17.35  $\mu\text{m}$  for transverse magnetic modes with  $p = 1$  to 3 and  $m = 230$  to 250 were aligned above the lasing spectrum. The linewidth of the modes was 0.16 nm, close to the spectral resolution of the spectrometer (0.1 nm).

The measured linewidth of the modes was 0.16 nm (Fig. 3e), close to the spectral resolution of the spectrometer (0.1 nm). This linewidth indicates that the quality factor of the modes was at least  $4 \times 10^3$ . Losses due to absorption, scattering due to potential contaminants in the drops, and perturbations in the size and shape of the drop can lead to degradation in the quality factor [5,16].

### 3.3 Blue-shift in emission wavelengths as the drops decreased in size

Figure 4a shows a series of emission spectra from drops possessing different sizes obtained at different positions in the channel (Fig. 2). The pulse energy of the pump beam was fixed at 0.24 mJ/pulse. We made three observations, as the drops decreased in size: (i) The wavelengths of the emitted light from the drops shifted from  $\sim 700$  nm to  $\sim 620$  nm as the radius of the drops decreased from 21  $\mu\text{m}$  to 7  $\mu\text{m}$ . (ii) The free spectral range (FSR)—measured from the spacing between consecutive modes in the emission spectrum—increased (Fig. 4b). (iii) The number of lasing modes decreased.

As the drops dissolved into the carrier fluid, three parameters changed: (i) The contrast in the refractive index between the drop and the carrier fluid decreased. (ii) The concentration of the dye solution in the drops increased. (iii) The radius of the droplet cavity decreased. We examine the effects of each below.

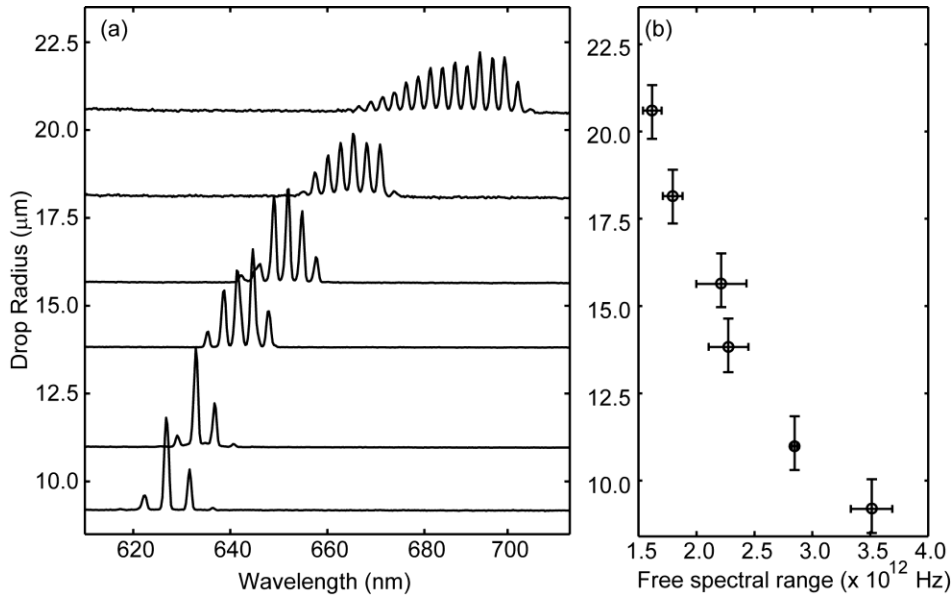


Fig. 4. a) Lasing spectra from drops possessing different radius  $R$ . The baseline value of each spectrum indicates the radius of the drop. The resolution of the spectrometer was 0.3 nm. Each spectrum is representative of emission from a single drop. b) Free spectral range (FSR) as a function of drop radius.

#### 3.3.1 Effect of decreased contrast in index of refraction between the drop and the carrier fluid

As benzyl alcohol dissolved into water, the refractive index of the continuous phase increased and that of the disperse phase decreased. Since the solubility limit of benzyl alcohol in water is 4%, the maximum refractive index of the continuous phase would be 1.34 (0.75% increase from 1.33). Water also dissolves in benzyl alcohol up to 8 wt %. The minimum refractive index of the drops would be 1.52 (1.3% decrease from 1.54). We also confirmed these values experimentally: the measured index of water saturated with benzyl alcohol was 1.34, and that of benzyl alcohol saturated with water was 1.52. Using the asymptotic formula in [29] (Appendix, Eq. (A5)), we estimated that the decrease in the contrast of refractive index between the drop and the carrier liquid would cause the positions of the WGMs to decrease  $\sim 5$  nm. This change was insignificant compared with the shift over 80 nm observed in Fig. 4.

#### 3.3.2 Effect of increased concentration of dye

The concentration of the rhodamine solution in the drops increased as the volume of the drops decreased. We measured the partition coefficient of rhodamine 640 perchlorate between

benzyl alcohol and water at equilibrium to be  $K_{bw} = [\text{dye}]_{\text{benzyl alcohol}}/[\text{dye}]_{\text{water}} \sim 20000$ . Because of this large value of  $K_{bw}$ , most of the dye molecules remained in benzyl alcohol. While we could not quantify the concentration of rhodamine solution inside the drops dynamically, the concentration should scale inversely with the volume of the drop. With the reduction in the volume of the drops in our experiments ( $V_{\text{initial}} \sim 125 V_{\text{final}}$ , corresponding to a decrease in radius of  $\sim 5$  fold), the highest concentration of rhodamine solution in the drop would be  $\sim 125$  mM, much lower than the solubility limit of rhodamine in benzyl alcohol (which we estimated to be at least 1 M). We did not expect, and did not observe, any aggregation or precipitation of dye molecules inside the drops as they decreased in volume.

To study the effect of different concentrations of dye solutions in the drops, we measured the emission spectra from drops at a fixed size (radius  $\sim 16.9 \mu\text{m}$ ) containing different concentrations of dye. We generated drops containing solutions of dye in benzyl alcohol that was saturated with water in a carrier fluid comprising water saturated with benzyl alcohol. These drops did not dissolve into the carrier fluid, and their size remained constant as they travelled downstream. Using this system, we were able to determine the effect of the concentration of the dye solution independent of the size of the drops. We found that the emission wavelengths increased from  $\sim 660$  nm to 700 nm as the concentration of rhodamine increased from 1 mM to 96 mM (data not shown). We therefore conclude that the increase in the concentration of the dye solution as the drops decreased in volume could not have caused the observed blue-shift in lasing wavelengths.

### 3.3.3 Effect of decreased radius of the drops

For WGMs of a fixed set of  $p$ ,  $m$ , and  $l$  numbers, the change in the wavelengths of WGMs is directly proportional to the change in the size of the cavity:  $\Delta\lambda_{p,m,l} / \lambda_{p,m,l} = \Delta R/R$  [4]. This relation does not apply to our system: the blue-shift in wavelengths would have been  $\sim 450$  nm, much larger than the observed 80 nm, when the radius of the drops decreased from  $21 \mu\text{m}$  to  $7 \mu\text{m}$ . We, therefore, believe the WGMs from drops with different sizes observed in our experiment belonged to different sets of  $p$ ,  $m$  and  $l$  numbers.

We attempt to provide a qualitative explanation for the changes in the wavelengths of emission based on the output power from the droplet cavities. In a microspherical cavity, light emitted from the gain medium either couples outside the cavity, or is absorbed by the medium. The efficiency ( $\beta$ ) of out-coupling of light from the cavity to free space can therefore be expressed as the ratio of the radiative quality factor  $Q_{\text{rad}}$  to the total quality factor  $Q_{\text{total}}$  of the cavity, which accounts for both radiative loss ( $Q_{\text{rad}}$ ) and absorption loss ( $Q_{\text{abs}}$ ) in the cavity as shown in Eq. (1) [13]:

$$\beta = \frac{Q_{\text{rad}}^{-1}}{Q_{\text{total}}^{-1}} = \frac{Q_{\text{rad}}^{-1}}{Q_{\text{rad}}^{-1} + Q_{\text{abs}}^{-1}} \quad (1)$$

The power  $P_o$  of lasing light coupled out of the cavity (i.e. the power that can be measured) can also be estimated following Eq. (6) in [13]:

$$P_o \sim \frac{V(R, \lambda)}{\lambda^3} g(\lambda) \beta(R, \lambda) \quad (2)$$

where  $V$  is the optical mode volume of the cavity,  $g$  is gain spectrum of the dye,  $R$  is the radius of the cavity, and  $\lambda$  is the wavelength of emission.

At wavelengths longer than the peaks of absorption and gain spectrum ( $\sim 600$  nm in our experiments, Fig. 3c), light at longer wavelengths experiences smaller absorption loss than light at shorter wavelengths; they are also less confined by a spherical cavity by total internal reflection. As a result, the efficiency of out-coupling of light from the cavity  $\beta$  increases with wavelength (Fig. 5a). On the other hand,  $g$  and  $V/\lambda^3$  decrease as wavelength increases (Fig. 5b). It is then trivial to show that  $P_o(\lambda)$ —the product of an increasing function and decreasing functions— must consist of a maximum (Fig. 5c). This maximum value is the peak

out-coupled laser power, and should correspond to the wavelengths of the observed lasing modes.

As the radius of the cavity decreases, the gain spectrum remains the same since it depends on the properties of the gain medium (dye) only. Mode volume  $V$  decreases as  $R$  decreases. Since smaller cavities are less able to confine light by total internal reflection than larger cavities, the out-coupling efficiency  $\beta$  increases as  $R$  decreases. The wavelength at which maximum output power occurs, therefore, shifts to short wavelengths as the cavity decreases in size (Fig. 5c). The wavelengths at which lasing can be observed should blue-shift correspondingly.

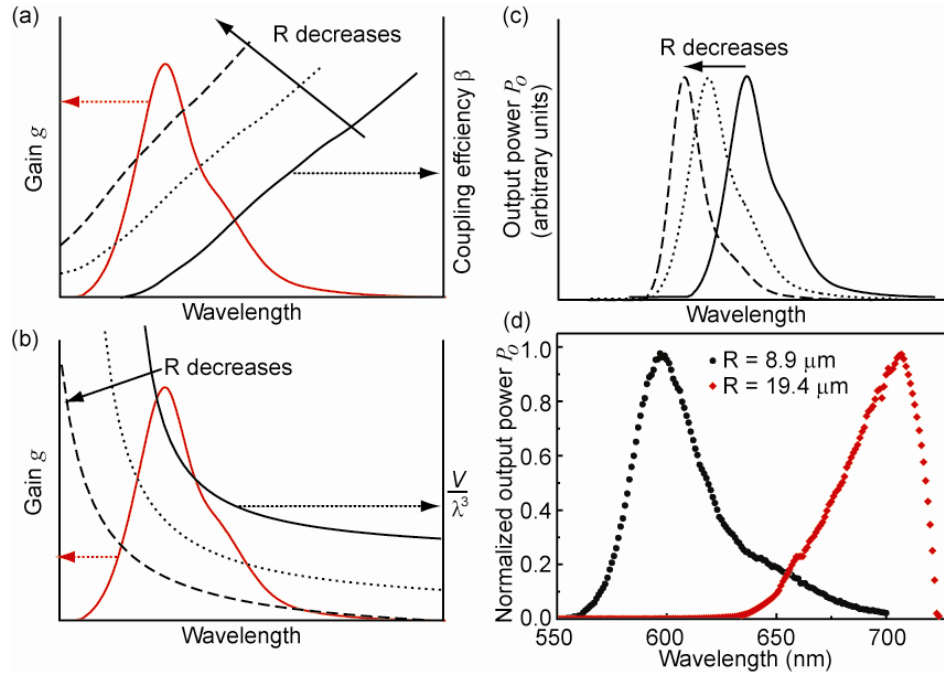


Fig. 5. (a) Schematic diagram showing the gain spectrum (red) and the out-coupling efficiency  $\beta$  (black) of light from the droplet cavity.  $\beta$  shifts to shorter wavelengths as the radius of the cavity  $R$  decreases. (b) Schematic diagram showing the gain spectrum (red) and  $V/\lambda^3$  (black), where  $V$  is the optical mode volume of the cavity.  $V/\lambda^3$  shifts to shorter wavelengths as  $R$  decreases. (c) shows a diagram of the output power from the droplet laser. Since the output power is proportional to the product of the gain spectrum, the mode volume, and the out-coupling efficiency, the emission peak shifts to shorter wavelengths as the radius of the cavity decreases. (d) shows the calculated output power envelopes for droplet cavities with  $R = 8.9 \mu\text{m}$  and  $R = 19.4 \mu\text{m}$  respectively. The shift in the peak output power from  $\lambda_{\text{peak}} \sim 700 \text{ nm}$  (for drops with  $R = 19.4 \mu\text{m}$ ) to  $\lambda_{\text{peak}} \sim 600 \text{ nm}$  (for drops with  $R = 8.9 \mu\text{m}$ ) was approximately equal to that observed in Fig. 4a.

Figure 5d shows the calculated output powers for two sizes of droplets using Eq. (2). From the calculations, the peak output power for drops with  $R = 19.4 \mu\text{m}$  occurred at about 700 nm; while that for drops with  $R = 8.9 \mu\text{m}$  occurred at about 600 nm. This blue-shift of 100 nm was close to that observed in Fig. 4a. The exact wavelengths of the peak output powers were different from the observed lasing wavelengths by  $\sim 20 \text{ nm}$ . We believe part of this difference originated from small errors in the values of the gain spectrum we used. The width of these calculated output power spectra was larger than that observed experimentally. For example, the calculation for drops at  $R = 8.9 \mu\text{m}$  implies the lasing power would be non-zero at wavelengths up to 680 nm, while the lasing modes in our experiment occurred between 620 nm and 640 nm only. This discrepancy arises from the fact that the calculations here did not account for effects such as mode clamping or mode competitions, which decrease the number of WGM modes allowed to lase.

The change in the size of the drops also explains the observed changes in the free spectral range (FSR) and the number of lasing modes. FSR scales inversely with the radius of the microcavity; modes in smaller drops have free spectral ranges larger than those in bigger drops. In addition,  $Q_{rad}$  is approximately proportional to the size parameter  $x$  of the cavity (defined as  $x = 2\pi R/\lambda$ ) (Appendix Eq. (A3), (A4) [13]). Modes in smaller drops thus have lower  $Q_{rad}$  than in bigger drops; the lower quality factors make these modes more difficult to lase. The number of lasing modes observed from smaller drops was, as a result, fewer than the number observed from bigger drops.

#### 4. Conclusions

We have demonstrated a droplet-based dye laser with a large range of tunability in its emitted wavelengths. Since a continuum of droplet cavities with continuously decreasing sizes was present in the channel, adjusting the position of the channel relative to the excitation beam allowed the selection and tuning of the emission wavelengths. The changes in emission wavelengths were due to changes in the size of the droplet cavities; effects due to changes in the indices of refraction and the concentration of the dye solution were insignificant. Lasing modes from the drops matched closely with the whispering gallery modes from spherical cavities. Possible deformations in the shape of the drops due to flow-induced shear in the microchannel did not affect the sphericity of the plane at which the whispering gallery modes were observed. We did not observe single-mode lasing in the smallest drops we generated ( $R \sim 7 \mu\text{m}$ ). It should, however, be possible to obtain single-mode lasing as the radius of drops decreased further [7].

Our method of generating droplet micro-cavities whose diameters decrease continuously was simple. It was more convenient than applying different rates of flow of the liquids. Applying different rates of flow usually requires time (up to tens of seconds or even minutes) for equilibration of flow after each change in the rate of flow. Many pairs of fluids that have limited mutual solubility can be used for our strategy, which does not rely on the characteristics of the drop generator, and should be compatible with any method for droplet generation. Further, it is possible to obtain drops of sub-micron sizes, if desired, and to increase the dissolution rate of the drops, by decreasing the volume fraction of the drops generated, or by incorporating additional continuous phase downstream.

The droplet cavities we described here can be useful as a tunable light source in combination with other microfluidic functionalities. In addition, with the increasing use of droplets as micro-compartments in microfluidic systems for studies in chemistry and biology [31], the investigation of optical properties of these droplets as optical microcavities can lead to the development of useful intra-cavity sensing schemes to monitor biochemical processes occurring inside the drops.

#### Appendix

Following definitions from [32], the transverse magnetic (TM) mode refers to the mode that has major radial component of electric field, and the eigenmode equation is:

$$\frac{[n_1 k R j_1(n_1 k R)]'}{n_1^2 j_1(n_1 k R)} = \frac{[n_2 k R h_1(n_2 k R)]'}{n_2^2 h_1(n_2 k R)} \quad (\text{A1})$$

Transverse electric (TE) mode has a vanished radial component, and the eigenmode is:

$$\frac{[n_1 k R j_1(n_1 k R)]'}{j_1(n_1 k R)} = \frac{[n_2 k R h_1(n_2 k R)]'}{h_1(n_2 k R)} \quad (\text{A2})$$

$R$  is the radius of the sphere,  $n_1$  is the refractive index of the sphere,  $n_2$  is the refractive index of the environment outside the sphere.  $k = 2\pi/\lambda$ .  $j_l$  and  $h_l$  are the spherical bessel and hankel functions. The radiative quality factor  $Q_{rad}$  of a particular eigenmode is:

$$Q_{rad} = \frac{\text{Re}[x]}{2 \text{Im}[x]} = \frac{n_1^2 (n_1^2 - n_2^2)^{1/2} \text{Re}[x]}{2n_2^2 \exp[-2T]} \quad (\text{A3})$$

where  $x$  is the size parameter  $x = 2\pi R/\lambda$ .  $T$  is a variable that depends on  $x$  weakly; the radiative quality factor  $Q_{rad}$  therefore scales linearly with the size parameter:

$$Q_{rad} \propto x \quad (\text{A4})$$

To match the lasing modes observed experimentally with theoretical WGM values, we derived the asymptotic solutions for mode order  $p$  and mode number  $m$  following [29]:

$$\lambda^{-1}(R, n_1, n_r, p, m) = \frac{1}{2\pi R n_1} \left[ m + \frac{1}{2} + 2^{-1/3} \alpha(p) \left(m + \frac{1}{2}\right)^{1/3} - \frac{L}{(n_r^2 - 1)^{1/2}} + \frac{3}{10} 2^{-2/3} \alpha^2(p) \left(m + \frac{1}{2}\right)^{-1/3} - 2^{-1/3} L \left(n_r^2 - \frac{2}{3} L^2\right) \frac{\alpha(p) \left(m + \frac{1}{2}\right)^{-2/3}}{(n_r^2 - 1)^{3/2}} \right] \quad (\text{A5})$$

where  $n_r = n_1/n_2$ ,  $L = n_r^{-1}$  for TM modes, and  $L = n_r$  for TE modes.  $\alpha(p)$  are the roots of the Airy function.

### Acknowledgements

We thank Howard Stone for helpful discussions. This work was funded by the Defense Advanced Research Projects Agency (DARPA) award number W911NF-07-10647. A portion of this work was supported by the National Science Foundation (NSF) NIRT award number ECCS-0708905. Device fabrication was performed at the Center for Nanoscale Systems at Harvard. R. Derda and Q. Quan contributed equally to this work.